JOURNAL OF MATERIALS SCIENCE **39** (2004) 6965–6973

Oxidation behaviour of a pressureless sintered AlN-SiC composite

D. SCITI, F. WINTERHALTER, A. BELLOSI
CNR-ISTEC, Institute of Science and Technology for Ceramics, Faenza, 48018, Italy
E-mail: dile@istec.cnr.it

The present study aims to investigate the oxidation behaviour of an AlN-SiC composite, pressureless sintered with the addition of Y_2O_3. Two main aspects are considered: (1) the evaluation of the oxidation kinetics in the temperature range 1300–1450°C for short term tests (30 h) and (2) the degradation of the flexural strength after oxidation at temperatures from 1000 to 1400°C for 100 h, in relationship with the microstructure of the exposed surfaces.

The material starts to oxidize notably at temperatures higher than 1300°C. The oxidation kinetics is parabolic in the temperature range 1350–1450°C, the oxidation products are dependent on temperature and exposure time and are mainly constituted by crystalline mullite and alumina.

The surface modification induced by long term oxidation does not affect mechanical strength until 1200°C, while after oxidation at 1400°C, the residual strength is about 25% of the starting one. These results are discussed in terms of the microstructure modifications induced by oxidation.

1. Introduction

Aluminum nitride and silicon carbide have attractive properties for many potential applications in the fields of electronics and at high temperatures. AlN possesses excellent physical properties such as high thermal conductivity, low thermal expansion and high electrical resistivity, while SiC is considered to be one of the most important structural ceramic due to its excellent high temperature properties.

Recently, the combination of these two materials has been studied in detail, since it was found that under proper sintering conditions, AlN and SiC form a 2H solid solution, which is very promising in terms of mechanical properties [1–9]. In contrast, few studies can be found on the oxidation behaviour of this composite [9–12] and there are still questions concerning the kinetics governing the oxidation process. This class of materials presents high oxidation resistance but oxidation behaviour depends on many factors, such as the test temperature, the AlN/SiC ratio, the sintering procedure, etc. It was reported, for instance [10], that for oxidation temperature <1550°C SiC-rich materials are more resistant, while at temperatures higher than 1550°C, AlN-rich materials show a better oxidation behaviour. The temperature strongly influences the types of oxidation products: tests carried out at temperatures lower than 1300°C led to the formation of cristobalite and aluminium oxynitride, while at higher temperatures or longer exposures, mullite was the main reaction product [11]. For SiC-rich composites and at temperatures in the range 1250–1370°C, a post-hipping treatment was observed to improve the resistance to oxidation of hot pressed composites [9]. However, further investigations are necessary to define the factors influencing the oxidation behaviour in order to exploit the potential of these materials for high temperature applications.

The studies found in literature were carried out on ceramics densified by hot pressing or by hot isostatic pressing. In this work, the oxidation behaviour was studied on a pressureless sintered AlN-SiC composite, in the temperature range 1000–1450°C. Moreover, the degradation of bending strength was studied after oxidation treatments for 100 h in the temperature range 1000–1400°C.

2. Experimental

2.1. Preparation of the materials

The raw powders used for the preparation of the composite materials are as follows:

AlN Grade C powder (H.C. Starck, Berlin, Germany) with d_{50} 2.29 μm, oxygen content of 1.8 wt% and specific surface area of 4.3 m^2/g; SiC BF-12 (H.C. Starck, Berlin, Germany) with mean particle size 0.23 μm, oxygen content of 0.88 wt% and specific surface area of 11.6 m^2/g; and Y_2O_3 grade C (H.C. Starck, Berlin, Germany) which was used as a sintering aid.

The following composition: 78.6 vol% AlN + 21.4 vol% SiC, to which 2 wt% of Y_2O_3 was added as sintering aid, was selected on the basis of preliminary experiments. The powder mixture was prepared by ball milling for 24 h in absolute ethanol using silicon nitride balls. The slurry was dried in a rotary evaporator and sieved.

Two different types of samples were prepared: (i) for short term oxidation tests (30 h), billets of 40 mm diameter and 10 mm thickness and (ii) for long term oxidation tests (100 h), sample bars with green dimensions 4 mm × 5 mm × 30 mm. All the green bodies were formed by uniaxial pressing followed by cold isostatic pressing under 350 MPa. They were then pressureless sintered in a 80 AlN/20 BN (wt%) powder bed at 1900°C for 70 min in flowing nitrogen. Sintered densities were measured using the Archimedes method.

2.2. Short term oxidation tests

From the sintered billets, rectangular plates of dimensions about 10 mm × 10 mm × 1 mm, were cut. One surface of each platelet was polished up to 6 μm with diamond paste. After the dimensions of the samples were measured, they were cleaned in acetone in an ultrasonic bath, then dried at 80°C for 12 h and carefully weighed (precision of 0.01 mg).

Short term oxidation tests were carried out on samples at 6 different temperatures (1000, 1200, 1300, 1350, 1400 and 1450°C) for different times from 2 to 30 h in order to evaluate the kinetics of the oxidation process. The experiments were carried out in an elevator furnace and the samples were introduced once the furnace had reached the selected temperature, in order to avoid the contribution of the oxidation during heating up. Surfaces and cross sections were analyzed by scanning electron microscopy and energy dispersive microanalysis (SEM-EDS). Crystalline phases were determined by X-ray diffraction and diffraction data were analysed using the PowderCell program [13] employing the March-Dollase orientation function [14].

2.3. Long term oxidation tests

Long term oxidation tests were carried out on bar specimens in a conventional furnace. The polishing treatment consisted of surface grinding with lapping machine in order to clean the surface from deposits deriving from sintering.

Polished bars were then oxidized in batches of five at 1000, 1200 and 1400°C for 100 h in laboratory air in order to study the degradation of the flexural strength as a consequence of the surface microstructure variation.

Before oxidation, the specimens were measured, cleaned in acetone in an ultrasonic bath, dried at 80°C for 12 h and weighed (precision of 0.01 mg).

Differently from the short term oxidation tests, the weight gain per unit surface area after oxidation $\Delta W/S$ (mg/cm^2) was recorded only at the end of the oxidation cycle; oxidized sample surfaces were analysed using X-ray diffraction.

Sample surfaces, polished cross sections and fracture surfaces were analyzed by scanning electron microscopy and energy dispersive microanalysis (SEM-EDS).

Fracture strengths of as-sintered and long term oxidized bars were measured using a four point bending jig with a lower span of 20 mm and an upper span 10 mm on an universal screw-type testing machine Zwick/Roell Z050 (Zwick/Roell, Germany) with a crosshead speed of 0.5 mm/min. Five bars were tested for each oxidation temperature.

3. Results

3.1. Microstructure of the starting material

There is not much porosity present in the sintered AlN/SiC composites, as shown in Fig. 1a and b. The relative density measured on sample bars after polishing is 99.7% of the theoretical density. The crystalline phases, determined from XRD analysis are: hexagonal AlN, β-SiC, $Y_3Al_5O_{12}$ (YAG). Extensive formation of AlN-SiC solid solutions can be ruled out, since β-SiC peaks are clearly visible in the XRD spectra (Fig. 2). However, comparing the relative intensities of the main peaks of AlN and SiC, the calculation of the corresponding amount of these phases, yields 7.5 vol% of SiC in the AlN-SiC mixture after sintering, which is considerably lower than its starting amount. Moreover, the variation of the cell parameters of AlN (compared to pure AlN) suggest that about 10 vol% of SiC has formed a solid solution with AlN. Owing to the relatively low temperature, the formation of solid solution was not completed; on the other hand a sintering temperature of 1900°C is a lower limit for AlN-SiC solid solution formation in the composition range of 20 to 80 wt% SiC [1].

As previously reported [6, 7], the densification of AlN-SiC mixtures is attributed to the formation of a liquid phase, that originates from reaction between the added Y_2O_3 and the Si- and Al-oxides which are present on the surface of SiC and AlN particles. In the sintered material, SiC and AlN grains are not distinguishable neither in secondary electron imaging, nor in back scattered electron imaging due to the very close atomic number, as revealed by Fig. 1b. The grains are surrounded by a brighter, gray grain boundary phase (Fig. 1b), that formed from the liquid phase during cooling from the sintering temperature. The composition of the grain boundary phase detected by EDS analyses is close to that of the YAG phase ($Al_5Y_3O_{12}$), however the presence of glassy yttrium silicates cannot be excluded. The micrographs of the microstructure suggest that the grains (either AlN or SiC) have dimensions in the 0.5–2.5 μm range.

3.2. Short term oxidation curves

No weight gain was observed after oxidation at 1000°C, a very low weight gain was measured in the range 1200–1300°C, whereas at temperatures above 1350°C the weight grain increased rapidly (Table I). Experimental data were fitted according to either a linear or a parabolic law, and the values of the parabolic/linear rate constants and of the fit goodness (R^2) are reported in Table I. The data from the test at 1300°C (not shown) are best fitted to a linear law, whilst the data from the tests carried out at 1350, 1400 and 1450°C, correspond to a parabolic rate law: $(\Delta W/S)^2 = Kt$ (see Fig. 3).

The thickness of the oxidised layer (Table I), measured on SEM micrographs of polished cross sections,

TABLE I Short term tests (1300–1450°C, 30 h); weight gain per unit surface area ($\Delta W/S$), kinetics and oxidation rate constants (K), fit goodness (R^2), thickness and composition of the oxide layer

T (°C)	$\Delta W/S$ (mg/cm^2)	Kinetics (K)	R^2	Layer thickness (μm)	Mullite/alumina vol. ratio	Mullite orientation	Al_2O_3 orientation
1300	0.65	Linear/3.1×10^{-9} g/cm^2 s^{-1}	0.965	10	80/20	111	No
1350	2.79	Parabolic/7.3×10^{-11} g^2/cm^4 s^{-1}	0.992	25	87/13	111	110
1400	10.75	Parabolic/1.1×10^{-9} g^2/cm^4 s^{-1}	0.996	190	90/10	001	110
1450	13.94	Parabolic/1.8×10^{-9} g^2/cm^4 s^{-1}	0.999	260	92/8	001	110

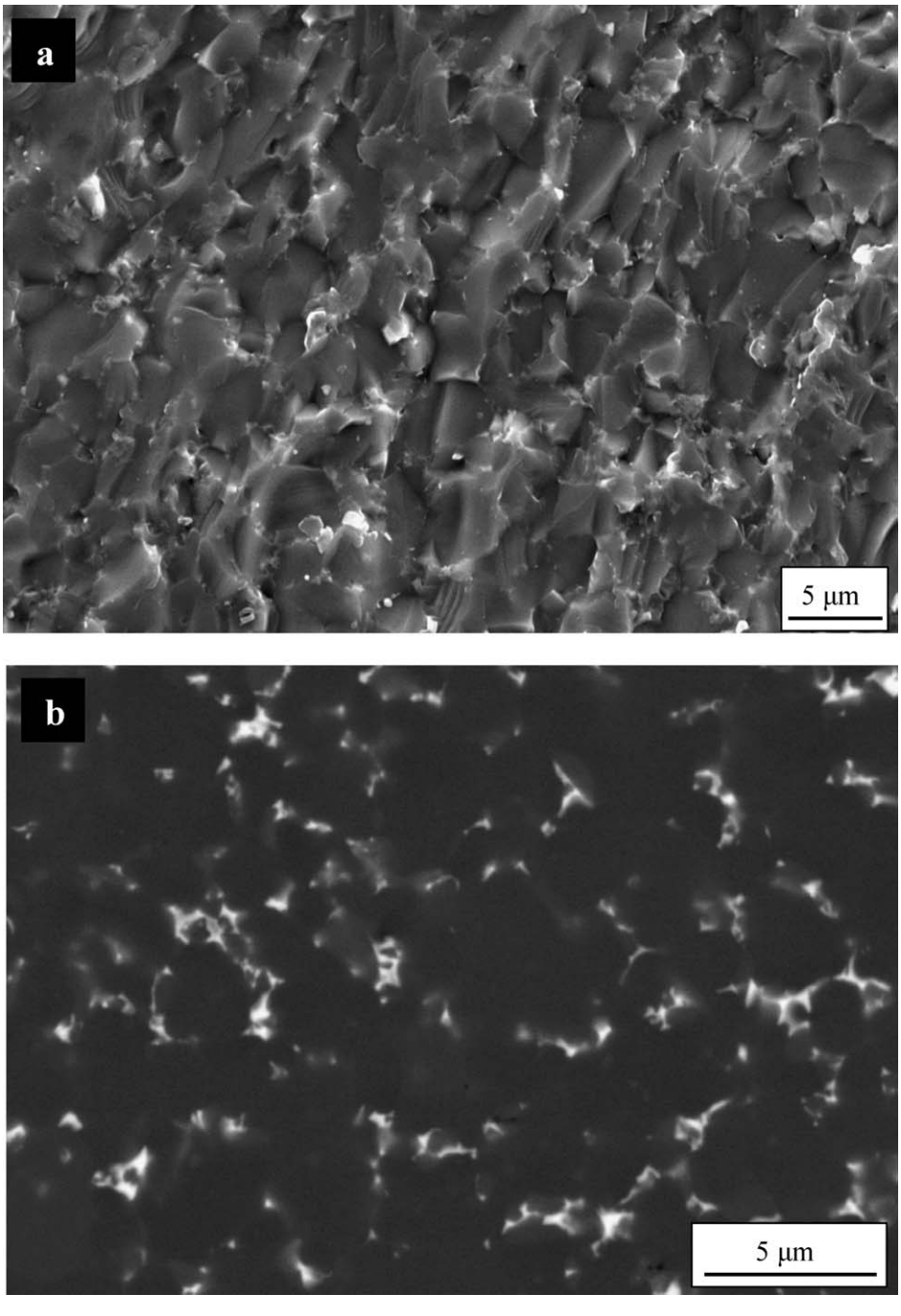

Figure 1 SEM micrographs of AlN-SiC sample: (a) fracture surface (secondary electron image) and (b) polished surface (backscattered electron image).

shows good agreement with weight-gain measurements. No measurable oxide layer was visible at the surface of the samples treated for 30 h in the temperature range 1000–1300°C. At 1300°C, the thickness was about 10 μm and it increased up to 260 μm at 1450°C.

A hot pressed material with the same relative amount of AlN and SiC, but without Y_2O_3, has a parabolic oxidation rate constant at 1350°C ranging between 1 and 3×10^{-10} g$^2 \cdot$ cm$^{-4} \cdot$ s^{-1} [11] which is about twice the value (7.3×10^{-11} g$^2 \cdot$ cm$^{-4} \cdot$ s^{-1}) calculated in the present study for the same oxidation temperature.

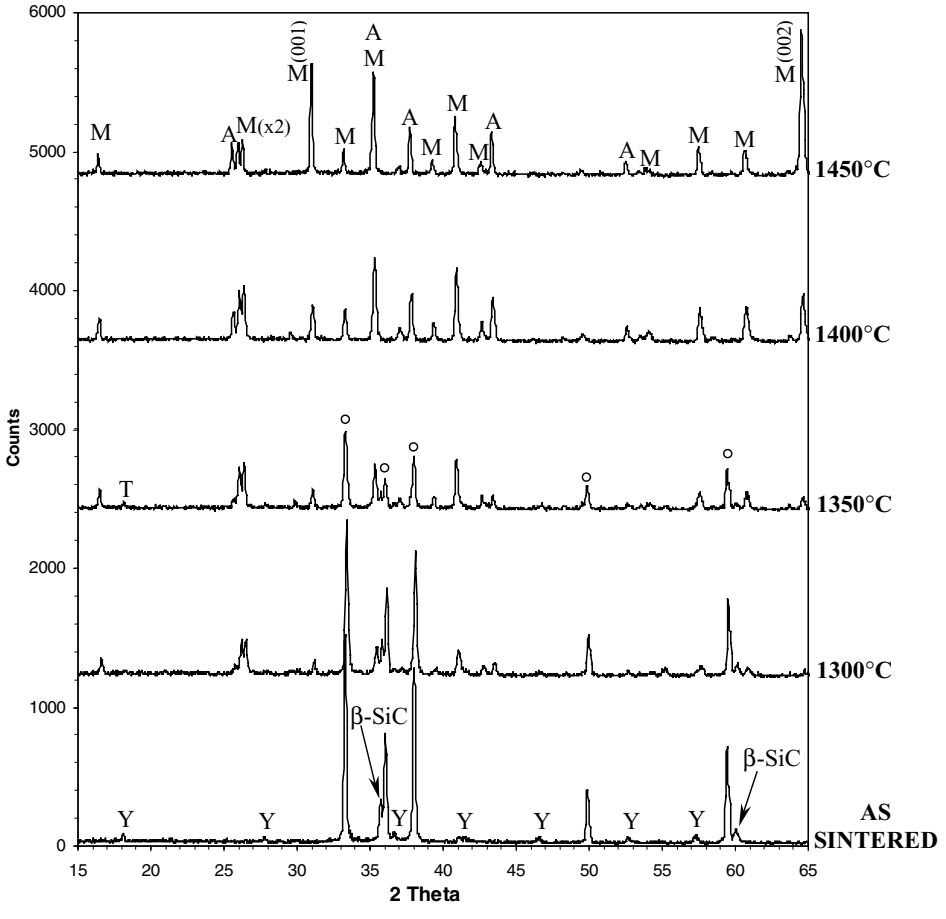

Figure 2 XRD spectra of sample surface as sintered and after the 30 h oxidation tests. Legend: M = mullite; A = α-Alumina; Y = YAG phase; T = trydimite; O = hexagonal AlN.

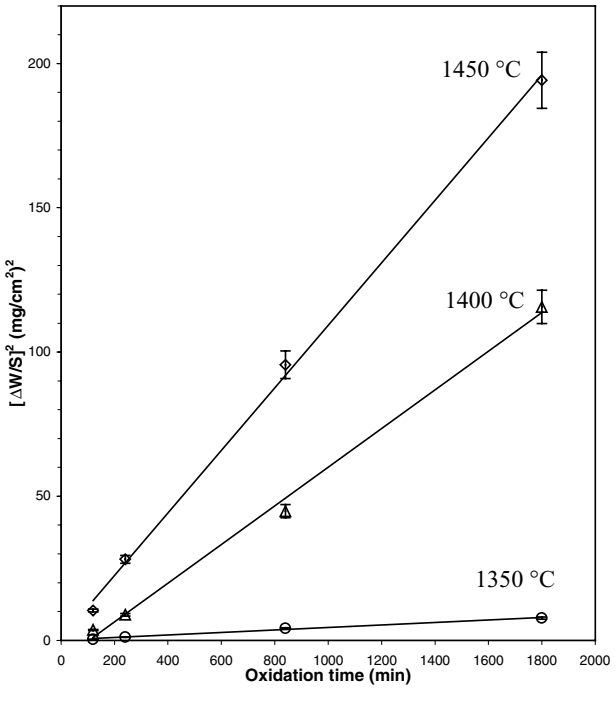

Figure 3 Squared weight gain per unit surface area vs. oxidation time in the range 1350–1450°C, and superimposition of fitting lines according to parabolic kinetics.

3.3. Microstructural characterization

XRD spectra of the surface of the sample after the 30 h oxidation tests are shown in Fig. 2. After oxidation at 1000°C, as well as the peaks of AlN and YAG, traces of crystalline corundum were detected; these were a little stronger after oxidation at 1200°C. At 1300 and 1350°C, peaks of AlN and YAG are still visible, due to the low oxide layer thickness. The main reaction products are mullite, α-alumina and traces of trydimite. At 1400 and 1450°C only mullite, α-alumina and traces of trydimite are visible, due to the masking effect of the thick oxide scale.

Mullite peaks show a preferential orientation along 111 planes after treatment at 1300 and 1350°C. At 1400°C, there is a change in the orientation of mullite from 111 to 001 (the angle between the two families of planes is about 30). The extent of orientation increases with temperature.

On the other hand, alumina is oriented along 110 planes after oxidation at $T > 1350$°C.

In order to determine the relative amounts of alumina and mullite in the product layer, the X-ray spectra were analysed using the PowderCell program, considering the March-Dollase orientation function to take into account of the orientation observed. The results, reported in Table I show that that the mullite content in the oxide layer increases with increasing oxidation temperature.

Observation of the surfaces after 30 h exposure at the selected temperatures (Fig. 4a–d) shows that the original surface is covered by crystals of newly formed phases, but this layer has some porosity. The crystals appear to be connected by glassy phase. Cracks were observed on the scales formed at $T > 1400$°C.

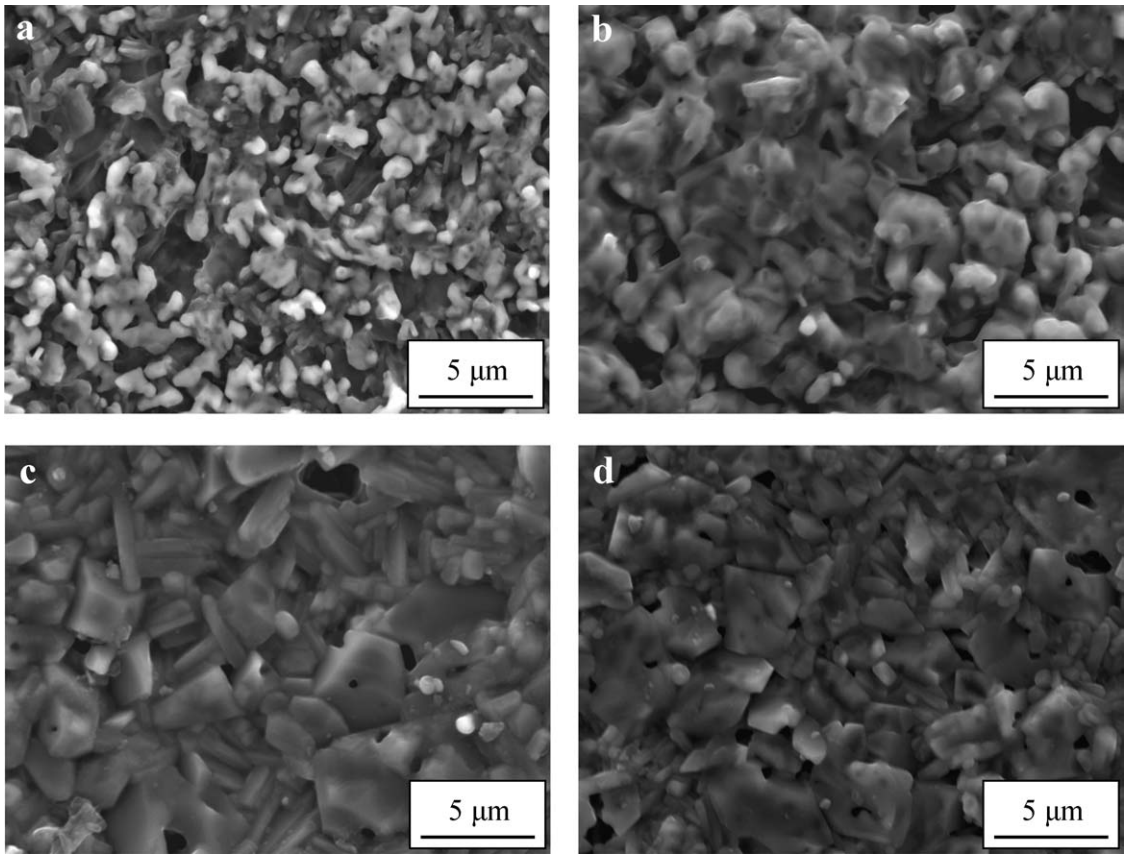

Figure 4 Surface of the oxidised samples after 30 h at (a) 1300°C, (b) 1350°C, (c) 1400°C and (d) 1450°C.

SEM analyses of the cross sections (Fig. 5a–d) highlight the increase of the oxide scale thickness, reported in Table I. Although some oxidation occurs at 1000 and 1200°C, the oxide scale is not clearly distinguishable from the unoxidised bulk. For samples treated at 1300, 1350 and 1400°C, the oxide scales are adherent to the bulk; the reaction interface is well defined and clearly separates the oxidation products from the unreacted bulk (an example is shown in Fig. 6a and b along with the EDS analysis of both parts).

A common feature, observed in the oxide scales, is the presence of a porosity gradient through the thickness of the scale. In the sample oxidised at 1350°C (Fig. 5b), a 10 μm thick portion of the scale next to the reaction interface contains approximately 5% of porosity; as the upper layer of the oxide scale is traversed, the porosity increases in amount and size. Through image analysis performed on SEM pictures it was calculated that in the upper layer porosity is about 25% and the mean pore size is about 1 μm. Whilst in the sample oxidised at 1400°C (Fig. 5c), the porosity looks more uniform, the layered structure of the oxide scale is particularly evident in samples oxidised at 1450°C (Fig. 5d). A detailed view, reported in Fig. 7, shows the presence of at least three layers. The first, close to the reaction interface, is a very porous layer (about 20 μm thick) with rounded or rod-like particles. According to EDS analyses, this layer is very poor in silicon, which probably indicates that once the silicon carbide oxidized, Si diffuses (probably as SiO) towards the upper part before reacting with α-alumina to form mullite.

The intermediate layer is 150 μm thick and has a porosity of about 16% and mean pore size 1 μm (pore range 0.6–8 μm). The outer layer (about 100 μm) has a porosity of about 30% and mean pore size 1.2 μm (pore range 0.9–11 μm).

Observation by back-scattered electrons of the outer part of the oxide scale (Fig. 8) reveals a microstructure comprising α-alumina grains and elongated mullite grains, which look "sintered" due to the effect of liquid phases. The morphological features show good wetting of α-alumina and mullite by these phases, which therefore result in a appearance similar to the "grain boundary phases" in sintered ceramics; their composition varies from a glassy silica phase to Y-containing glassy silicates. Large pores are also present.

The presence of Y_2O_3 as a sintering aid in the starting material, does not seem to influence the oxidation behaviour. The YAG phase peaks, detected by X-ray in the starting samples, were not found after oxidation cycles, due to the masking effect of the oxide scale. Yttrium is present in the oxide scale in randomly distributed pockets of glassy Y-silicates. Moreover, previous studies on AlN oxidation behaviour up to 1390°C, confirmed that pure AlN and Y_2O_3-doped AlN have almost the same behaviour in terms of oxidation kinetics and oxidation products [15].

3.4. Strength degradation after long term tests

The 100 h oxidation tests were mainly performed to investigate the change in flexural strength in comparison

TABLE II Long term tests at (1000, 1200 and 1400°C, 100 h); weight gain per unit surface area ($\Delta W/S$) and thickness and composition of the oxide layer, 4-pt plexural strength of as-sintered and oxidized samples

Sample	Oxidation temperature (°C)	$\Delta W/S$ (mg/cm^2)	Layer thickness (μm)	Crystalline phases	Flexural strength (MPa)
As sintered	–	–	–	AlN; β-SiC; YAG; 10 vol% 2H solid solution	379 ± 58
Oxidised	1000	−0.03	0	AlN; β-SiC; YAG; traces: α-alumina	283 ± 44
Oxidised	1200	0.38	0	AlN; α-alumina	266 ± 44
Oxidised	1400	28.75	450	α-alumina; traces: mullite	88 ± 11

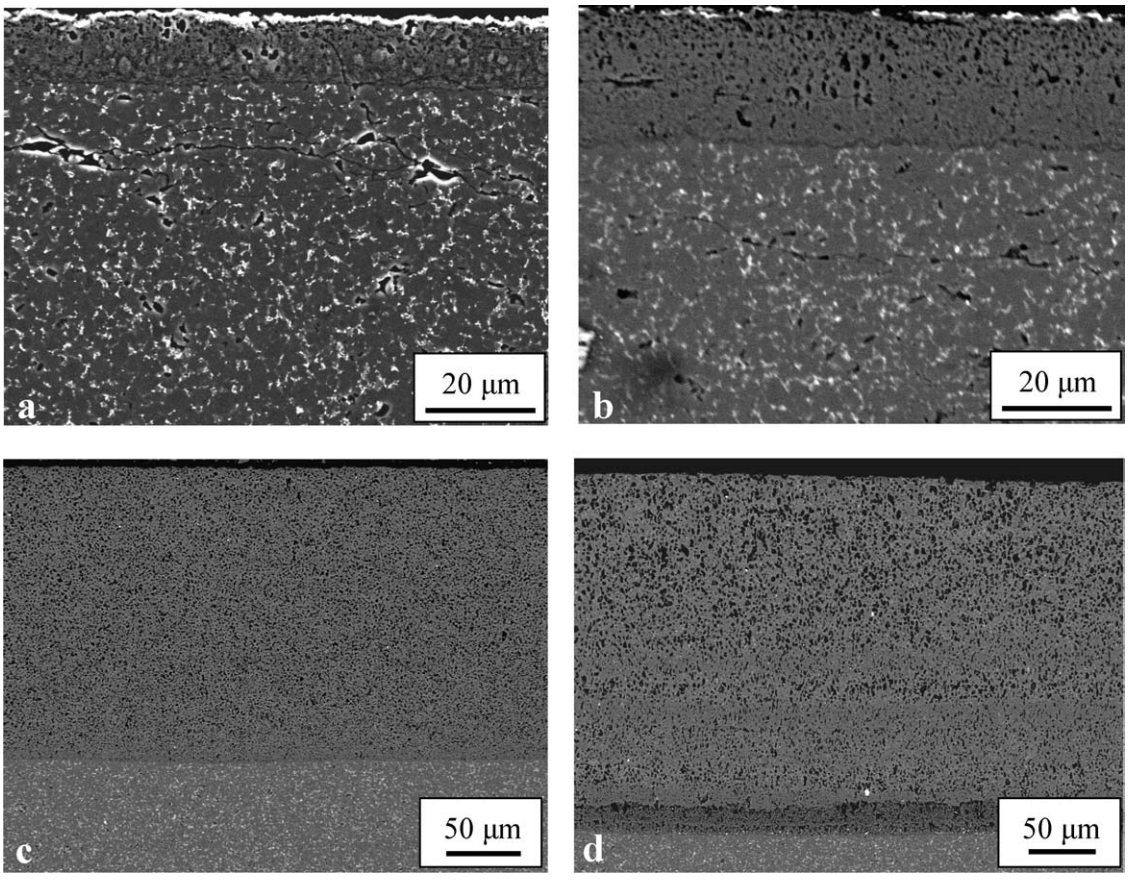

Figure 5 Cross sections of the oxidised samples after 30 h at (a) 1300°C, (b) 1350°C, (c) 1400°C and (d) 1450°C.

to the as sintered material. However microstructural characterization was performed as well.

After the long term tests, weight changes, reported in Table II, reveal that the weight gain is appreciable only at temperature above 1200°C. Correspondingly, a clear oxide layer is revealed on SEM micrographs only after oxidation at 1400°C and this oxide scale reaches a thickness of 425 μm. The main oxidation product revealed by XRD is α-alumina which starts to nucleate during treatment at 1000–1200°C, while mullite peaks are visible only after oxidation at 1400°C. Details of the cross section of the sample oxidized at 1400°C (not shown), evidence the same layered structure as described for the short term samples oxidized at 1450°C, i.e., an intermediate porous layer, between the bulk and the oxide scale.

The fracture strength values for samples oxidized at various temperatures are presented in Table II. Compared to the as sintered material, strength degradation is very limited after oxidation tests at 1000 and 1200°C, whilst it is significant after the oxidation at 1400°C. The fracture originates from porosity and defects located in the brittle surface scale.

4. Discussion

There are few works in the literature concerning the oxidation behaviour of AlN-SiC composites. All the studies [11] report the formation of a scale of mullite at temperatures above 1300°C, through different mechanisms. Also, the kinetics itself are not clear. Xu *et al.* [12] assumed a parabolic reaction rate, while Landon *et al.* [10] could not apply any kinetic law to their experimental data.

The composites are composed of two oxidizable phases, where AlN is usually less stable than SiC in oxygen-rich atmosphere at high temperatures [12]. At temperatures above 600°C, monolithic AlN reacts with oxygen forming alumina which can be amorphous at $T < 1000$°C and becomes crystalline corundum at $T > 1000$°C. Different kinetic models have been proposed for the oxidation of AlN depending on time, temperature, oxidizing atmosphere and characteristics

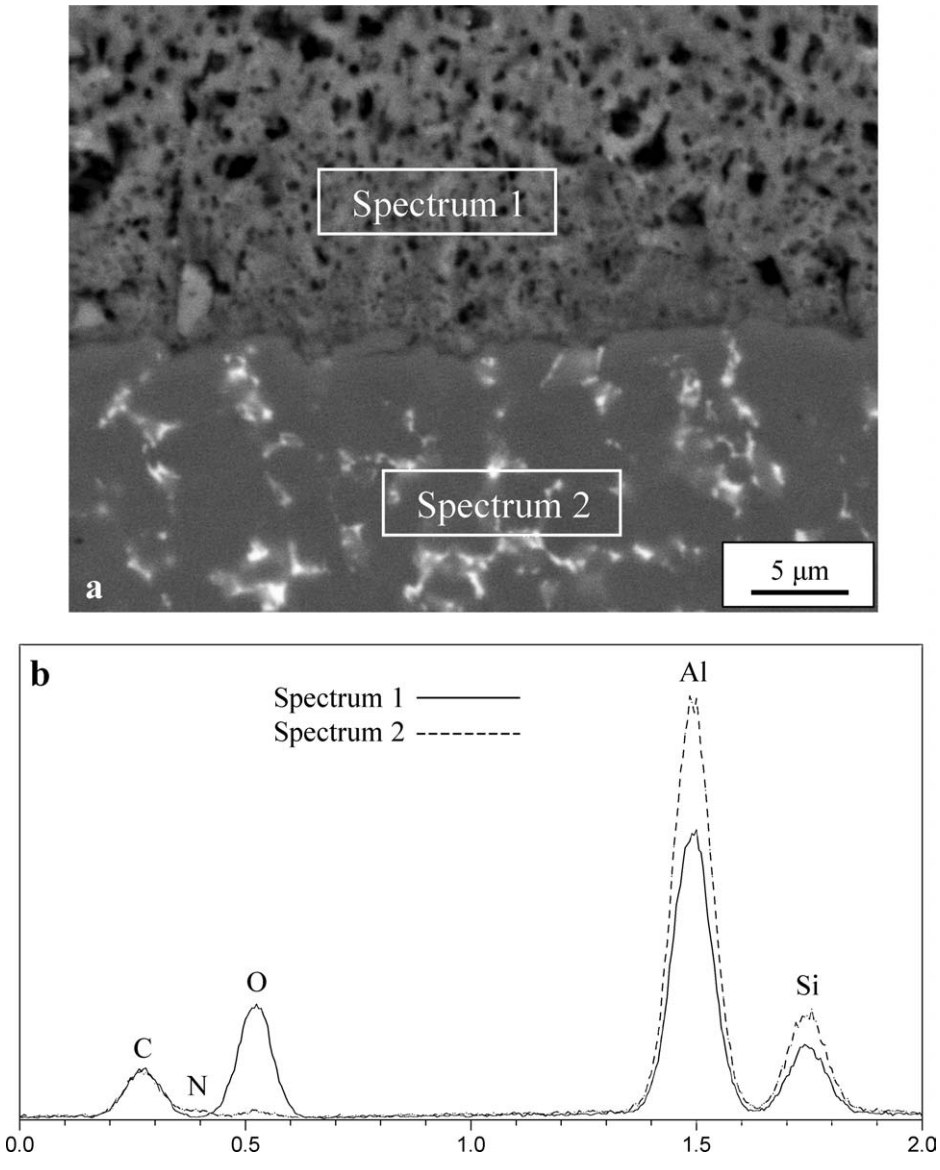

Figure 6 (a) Reaction interface after oxidation at 1400°C and (b) EDS analysis.

of the samples. Parabolic behaviour is reported by Lavrenko *et al*. [16], and oxygen diffusion is indicated as the rate controlling mechanism. In contrast, in the work of Bellosi *et al*. [15], the alumina scale was found to be non protective, due to porosity, and consequently the kinetic law was linear.

On the other hand SiC is a very stable phase due to the development of a SiO_2 protective layer. As oxygen permeability through the SiO_2 scale is very low, the rate controlling mechanism of oxidation is diffusion of oxygen through the oxide scale, which accounts for the parabolic kinetics. When AlN and SiC are combined together in the composites, the two main oxidation products, alumina and silica can further react forming mullite according to the reaction:

$$3Al_2O_3 + 2SiO_2 \rightarrow 3Al_2O_3{\cdot}2SiO_2 \qquad (1)$$

Alternatively, as proposed by Lavrenko *et al*. [11], the first stage of AlN oxidation would be characterized by the formation of $Al_{10}N_8O_2$, that afterwards forms mullite as a result of its reaction with silica.

In presence of AlN-SiC solid solutions, Xu *et al*. [12] proposed a two step mechanism involving at first the formation of Si-Al-O-Ns and carbon (graphite), and then the final oxidation of the Si-Al-O-Ns to mullite and silica. In both the second oxidation steps above described i.e., the formation of mullite from reaction of $Al_{10}N_8O_2$ with SiO_2 and the oxidation of sialon to mullite and silica, the nitrogen outward diffusion should be as limiting as the oxygen inward diffusion for AlN-rich solid solutions [11, 12]. Whilst an alumina scale can be protective or not, a mullite scale was usually found to be protective for AlN-SiC and Al_2O_3-SiC composites [17] even if the extent of protection is still a matter of debate.

In the present work, experimental results indicate that the oxidation proceeds mainly through formation of alumina and silica (in the form of trydimite) and after treatment at temperatures higher than 1300°C, mullite forms according to reaction (1). This is suggested because aluminum oxynitride was never detected in the oxidation product and the amount of AlN-SiC solid solutions in the as sintered material is very low, consequently its oxidation cannot be the rate-controlling step for the whole oxidation process.

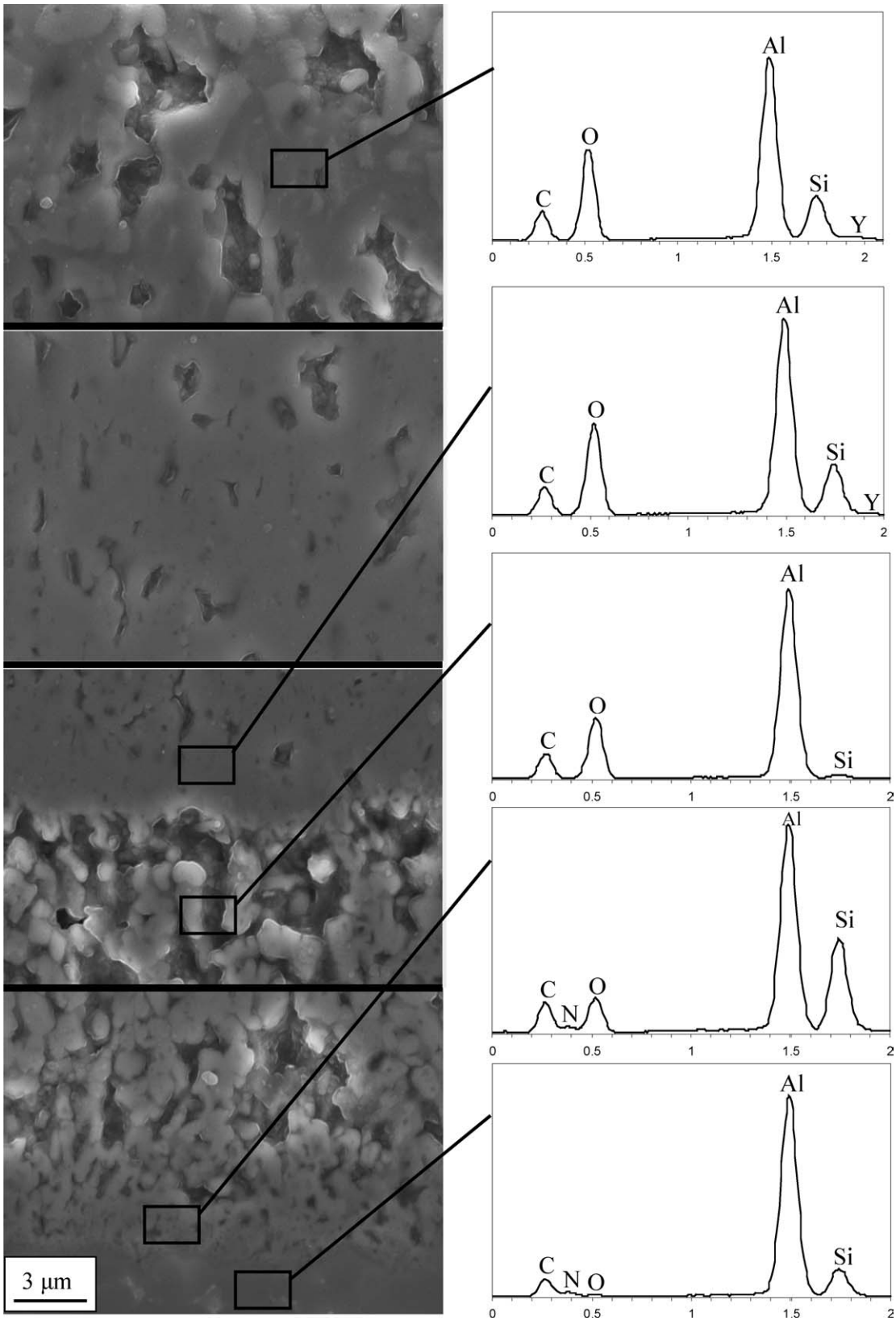

Figure 7 Layered structure in the oxide scale of sample oxidised at 1450°C/30 h.

Since the starting material has an AlN-rich composition, the lack of silica does not allow a complete transformation of alumina into mullite. As only traces of crystalline silica were observed at temperatures lower than 1300°C, it is likely that SiC oxidation gives rise to gaseous Si-O species that diffuse towards the surface.

The parabolic kinetics found in the range 1350–1450°C confirm that the mullite-alumina scale is protective and, therefore, the rate controlling mechanism is likely to be diffusion of oxygen towards the reaction interface.

At 1300°C, deviation from a parabolic behaviour could be due to the non-protective nature of the oxidation product because of the low thickness and high porosity of the surface scale and the larger amount of alumina in the scale.

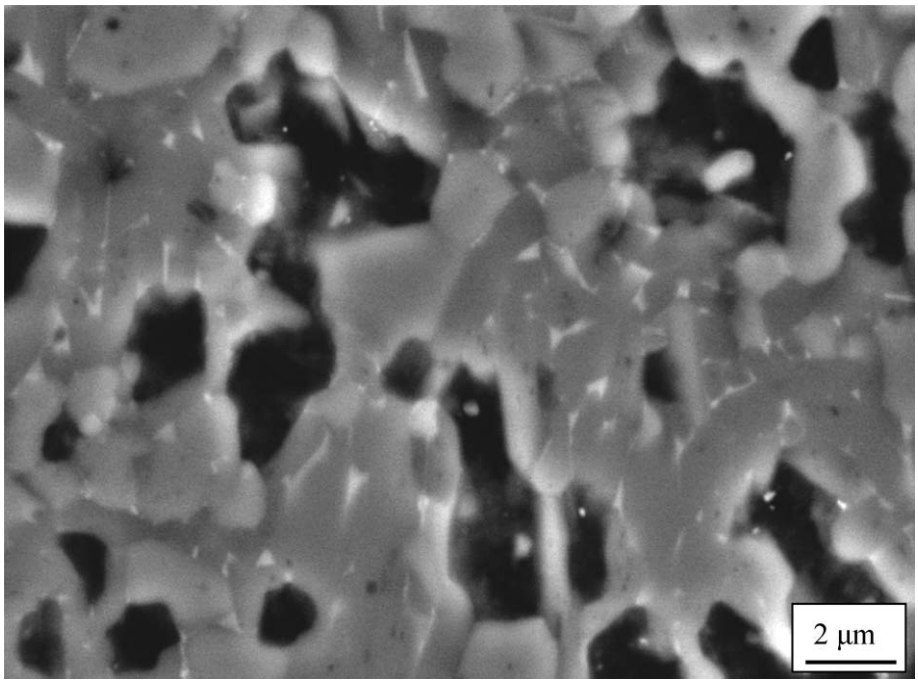

Figure 8 External part of the oxide scale observed by back-scattered electrons in sample oxidised at 1450°C for 30 h.

5. Conclusions

The oxidation of a pressureless sintered AlN-SiC composite, studied both for short term and long term exposure in air, starts at 1300°C. However, the formation of a thick oxide scale occurs only for temperatures above about 1350°C. The oxide scale is formed mainly by mullite and α-alumina crystals. Traces of trydimite were detected up to 1350°C. The oxide scales present a gradient of porosity from the reaction interface towards the surface and a layered structure appears on specimens oxidized at temperature higher than 1400°C. The oxidation kinetics are parabolic in the temperature range 1350–1450°C, indicating that diffusional processes are limiting the oxidation. At lower temperature, the linear kinetics indicate that the process is governed by chemical reaction at the interface.

Flexural strength tests carried out on bars after oxidation at 1000, 1200 and 1400°C for 100 h, evidenced that, compared to as sintered bars, the strength degradation is very limited in samples oxidized at 1000 and 1200°C, while it is relevant in samples oxidized at 1400°C.

Acknowledgements

The work is supported by the European Project Research Training Network HPRN-CT-2000-00044 "Composite Corrosion". The research contract of F. Winterhalter is funded by the same Project.

The authors wish to thank their colleagues: S. Guicciardi and C. Melandri for the measurement of mechanical properties, D. Dalle Fabbriche and A. Balbo for their help in leading the oxidation tests and S. Tarlazzi and G. Celotti for the X-ray characterization.

References

1. J.-L. HUANG and J.-M. JIH, *J. Mater. Res.* **10** (1995) 651.
2. W. RAFANIELLO, M. R. PLICHTA and A. V. VIRKAR, *J. Amer. Ceram. Soc.* **66**(4) (1983) 272.
3. J.-F. LI and R. WATANABE, *J. Mater. Sci.* **26** (1991) 4813.
4. A. H. LUBIS, N. L. HETCH, G. A. GRAVES and R. RUH, *J. Amer. Ceram. Soc.* **82**(9) (1999) 2481.
5. Y. PAN, S. TAN, D. JIANG, J. QIU, M. KAWAGOE and M. MORITA, *J. Mater. Sci.* **34** (1999) 5357.
6. J.-F. LI and R. WATANABE, *J. Ceram. Soc. Jpn., Int. Ed.* **102** (1994) 724.
7. Y. R. XU, A. ZANGVIL, M. LANDON and F. THEVENOT, *J. Amer. Ceram. Soc.* **75**(2) (1992) 325.
8. J.-L. HUANG and J.-M. JIH, *ibid.* **79**(5) (1996) 1262.
9. Y.-B. PAN, J.-H QIU, M. KAWAGOE, M. MORITA, S.-H. TAN and D.-L. JIANG, *J. Eur. Ceram. Soc.* **9** (1999) 1789.
10. M. LANDON, P. GOEURIOT and F. THEVENOT, *ibid.* **8** (1991) 279.
11. V. A. LAVRENKO, M. DESMAISON-BRUT, A. D. PANASYUK and J. DESMAISON, *ibid.* **18** (1998) 2339.
12. Y. XU, A. ZANGVIL and R. RUH, *J. Amer. Ceram. Soc.* **78**(10) (1995) 2753.
13. W. KRAUS and G. NOLZE, "PowderCell for Windows 2.1" (Federal Institute for Materials Research and Testing, Berlin, Germany, 1998).
14. W. A. DOLLASE, *J. Appl. Crystall.* **19** (1986) 267.
15. A. BELLOSI, E. LANDI and A. TAMPIERI, *J. Mater. Res.* **8**(3) (1993) 565.
16. V. A. LAVRENKO and A. F. ALEXEEV, *Ceram. Int.* **9**(3) (1983).
17. K. L. LUTHRA and H. D. PARK, *J. Amer. Ceram. Soc.* **73**(4) (1990) 1014.

Received 26 September 2003
and accepted 3 June 2004